CrossMark

In-Situ Systematic Error Correction for Digital Volume Correlation Using a Reference Sample

B. Wang[1] · B. Pan[1] · G. Lubineau[2]

Abstract The self-heating effect of a laboratory X-ray computed tomography (CT) scanner causes slight change in its imaging geometry, which induces translation and dilatation (i.e., artificial displacement and strain) in reconstructed volume images recorded at different times. To realize high-accuracy internal full-field deformation measurements using digital volume correlation (DVC), these artificial displacements and strains associated with unstable CT imaging must be eliminated. In this work, an effective and easily implemented reference sample compensation (RSC) method is proposed for *in-situ* systematic error correction in DVC. The proposed method utilizes a stationary reference sample, which is placed beside the test sample to record the artificial displacement fields caused by the self-heating effect of CT scanners. The detected displacement fields are then fitted by a parametric polynomial model, which is used to remove the unwanted artificial deformations in the test sample. Rescan tests of a stationary sample and real uniaxial compression tests performed on copper foam specimens demonstrate the accuracy, efficacy, and practicality of the presented RSC method.

✉ B. Pan
 panb@buaa.edu.cn

✉ G. Lubineau
 gilles.lubineau@kaust.edu.sa

1 Institute of Solid Mechanics, Beihang University, Beijing 100191, China

2 Physical Science and Engineering Division, COHMAS laboratory, King Abdullah University of Science and Technology (KAUST), Thuwal 23955-6900, Saudi Arabia

Introduction

As an image-based experimental technique, digital volume correlation (DVC) [1–4] retrieves full-field internal deformation by comparing volume images at different states recorded by a volumetric imaging device. Basically, DVC measurement involves two steps [2]: volume image acquisition using a 3D imaging device, followed by internal displacement tracking using a 3D image registration algorithm. Analogous to its 2D counterpart (i.e., 2D digital image correlation [5]), the accuracy and precision of DVC measurements therefore highly depend on the following two aspects: (1) the texture, imaging quality and fidelity of the volume images; and (2) the performance of the sub-voxel displacement registration algorithm. The continual refinement of correlation-based image registration algorithms now allows sub-voxel registration with a displacement accuracy higher than 0.005 voxels for computer-simulated volumetric images [6, 7], which are free of artifacts commonly encountered in X-ray computed tomography (CT). However, it should be emphasized that when dealing with real volume images, high-accuracy DVC measurement cannot be realized without eliminating systematic errors induced by an imperfect and unstable volumetric imaging system.

Due to their easy accessibility and wide applicability, laboratory X-ray CT scanners have been the most commonly used 3D imaging devices in various DVC applications. Though an advanced laboratory X-ray CT facilitates the acquisition of high-quality volume images with high contrast and spatial resolution [8–11], it is not without its shortcomings. In fact, various noise and image artifacts inevitably occur during CT scan [12, 13]. Among these error sources, the self-heating effect of X-ray CT devices has been identified as the factor most detrimental to DVC measurement [14, 15]. This is because the spatial position of an X-ray emission point may undergo continual and slight change during scans due to the heat generated by the X-ray tube,

which changes the imaging geometry of the CT device and induces both translation and dilatation (i.e., artificial displacements and strains) in reconstructed volume images [16, 17].

Very recently, the systematic error in DVC measurements associated with the self-heating effect of a laboratory X-ray CT scanner was carefully examined by the present authors [15]. By characterizing the relationship between the artificial strain and operation time of the X-ray tube, a strain-error correction method based on a pre-established artificial strain-time curve was presented. However, this correction method has several obvious limitations, including: 1) heavy dependence upon time and scanning settings; and 2) time delay due to ex-situ pre- or post-calibration procedures. For these reasons, an *in-situ* systematic error correction method that will contribute to the optimal use of DVC is highly desirable.

Inspired by the reference sample compensation (RSC) method developed in 2D–DIC [18], we propose an effective and easily implemented RSC method for *in-situ* systematic error correction in DVC using a laboratory X-ray CT system. The key of the proposed RSC method lies in the use of a stationary reference sample, which is placed beside the test sample to record the artificial displacement maps associated with the self-heating effect of the CT scanner. The artificial displacement fields are then fitted with parametric polynomials, which can be used to eliminate the undesired artificial displacement field in the test sample. In the remainder of this paper, the relationship between the self-heating effect and the induced systematic errors in DVC measurement is theoretically analyzed first. Then the basic principle of the proposed RSC method is detailed. Finally, a series of rescan tests and a stepwise uniaxial compression test using copper foam specimens were performed to demonstrate the efficacy and practicality of the presented RSC method.

Reference Sample Compensation Method for DVC

The Self-Heating Effect and its Influences on the Imaging Geometry of X-Ray CT

As reported previously [19–21], the self-heating effect of an X-ray CT system can change the spatial position of its X-ray emission point, which in turn induces artificial displacements and strains in reconstructed volume images. These artificial deformations can be detected by a DVC algorithm, and thus corrupting the desired deformation caused by physical loading. To realize high-accuracy interior deformation measurement, these artificial deformations should be eliminated.

For the convenience of theoretical analysis, here we show only the in-plane demonstration to simplify the complex spatial geometric changes. The influence of the self-heating effect on imaging geometry, along with motions of the emission point, is schematically shown in Fig. 1. Throughout the following theoretical derivation, the origin of the sample coordinate system is defined as the center of rotation, and the x-axis is set as the direction of the X-ray optical axis. D_0 and d_0 are the preset source-object distance and source-camera distance, respectively, and D_1 and d_1 are their thermally-changed counterparts.

In Fig. 1, the thermal shifts of the emission point can be decomposed into motions perpendicular to and along the X-ray beam. The y-directional drift Δy of the emission point is equivalent to the motion of the sample in the opposite direction, thus only inducing rigid-body translation within the reconstructed volume images. The corresponding artificial displacement component v_1 can be written as

$$v_1 = \frac{D_0 - d_0}{d_0} \cdot \Delta y \tag{1}$$

The above expression indicates that the artificial translation in the volume image relies on three factors: y-directional thermal drift Δy during image acquisition, the preset source-object distance d_0, and the source-camera distance D_0.

Furthermore, due to the assembly constraints of mechanical components within a CT tube, the emission point continuously gets close to the sample because of the self-heating effect during a practical CT scan [14]. This leads to motions of emission point along the positive x-axis. As such, the reduced source-object distance increases the magnification of the imaging geometry from D_0/d_0 to D_1/d_1, giving rise to uniform dilatational strains within the reconstructed volume images:

$$\varepsilon = \frac{D_1/d_1}{D_0/d_0} - 1 = \frac{D_0 - \Delta x}{d_0 - \Delta x} \cdot \frac{d_0}{D_0} - 1 \tag{2}$$

It can be concluded that the thermally-induced dilatational strain in the volume image is directly related to the selected source-object distance d_0, the source-camera distance D_0, and the x-directional thermal drift Δx during image acquisition. Existing research has claimed that the artificial strain can reach 4000 microstrain due to the self-heating effect [14], which is detrimental to quantitative displacement measurement using DVC.

To quantitatively examine the influences of the self-heating effect on DVC measurements, Table 1 lists the scan settings of the Skyscan 1172 X-ray Micro-CT system employed in this
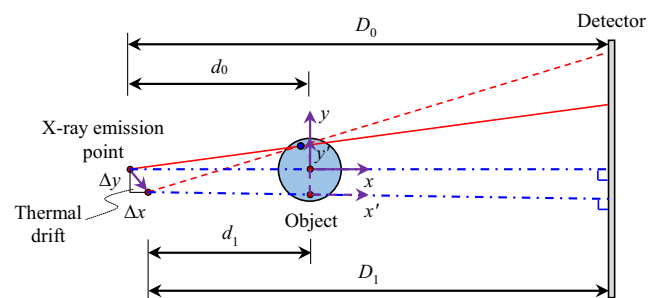

Fig. 1 Thermal drift of emission point due to the self-heating effect of a lab X-ray CT changes its imaging geometry

Table 1 Scan settings of Skyscan 1172 X-ray Micro-CT system

	Spatial sampling grid (pixel)	1000 × 668	2000 × 1336	4000 × 2672
Voxel size (µm)		2.00–27.14	1.00–13.43	0.50–6.72
Source-object distance d_0 (mm)		19.14–259.95	19.14–257.37	19.14–257.37
Source-camera distance D_0 (mm)		342.94	342.94	342.94

work. During a CT scan, the selected voxel size (the physical dimension of one voxel in the volume image) and spatial sampling grid are closely related to specific values of d_0 and D_0. In cases of higher magnification, the source-object distance would be shorter, as the source-camera distance is fixed. Thus, the same thermal motion along the x-axis can lead to larger artificial dilatational strains.

In practice, the generated heat inside an X-ray CT tube may also slightly change the direction of the X-ray beam during CT scan, as illustrated in Fig. 2. In this case, artificial rigid-body rotation and non-uniform deformation would be present in the volume images, about which corresponding theoretical analyses are detailed in the Appendix. However, the artificial rotation components identified in previous experiments [15] are relatively small and have negligible influence on strain results. Also, the induced non-uniform deformations are generally presented as random intensity changes rather than global bias errors, as discussed in the Appendix.

Therefore, it can be concluded that the systematic errors in DVC measurement due to the self-heating effect of an X-ray CT system consist of two major components, i.e. artificial translation and dilatational strain, and a minor component, i.e. artificial rotation. These systematic errors cause global bias in DVC-measured displacements and strains, and thus should be corrected or compensated to recover the desired deformation results.

Reference Sample Compensation Method

To eliminate the above-mentioned artificial displacements and strains due to the self-heating effect, a reference sample compensation (RSC) method is proposed to correct the systematic error in DVC. A schematic diagram showing the principle of the RSC method is presented in Fig. 3. In practical implementation, a smaller stationary reference specimen without external loading is placed beside the tested sample on the rotation stage. Note that the gap between them should be large enough to ensure the reference sample is free from any external loadings during the entire loading process.

During image scanning, the volume images of the reference sample just record the imaging errors due to the self-heating effect of the CT system. Then, a flexible and accurate subvolume-based DVC method using an advanced inverse-compositional Gauss-Newton algorithm and a novel layer-wise reliability-guided displacement tracking strategy [22] is employed to measure the thermally-induced artificial displacement fields in the reference sample. To extract the deformation components from the measured displacement fields, the following expression for displacement decomposition is employed:

$$\begin{bmatrix} u_{ri} \\ v_{ri} \\ w_{ri} \end{bmatrix} = \begin{bmatrix} t_x \\ t_y \\ t_z \end{bmatrix} + \underbrace{\begin{bmatrix} 0 & -\omega_z & \omega_y \\ \omega_z & 0 & -\omega_x \\ -\omega_y & \omega_x & 0 \end{bmatrix}}_{Rotation} \cdot \begin{bmatrix} x_{ri} \\ y_{ri} \\ z_{ri} \end{bmatrix} + \underbrace{\begin{bmatrix} \varepsilon_x & 0 & 0 \\ 0 & \varepsilon_y & 0 \\ 0 & 0 & \varepsilon_z \end{bmatrix}}_{Dilatation} \cdot \begin{bmatrix} x_{ri} \\ y_{ri} \\ z_{ri} \end{bmatrix} \tag{3}$$

where u_{ri}, v_{ri}, and w_{ri} are the respective x-, y-, and z-directional displacement components of the ith calculation point; x_{ri}, y_{ri}, and z_{ri} are the x, y, and z coordinates of the ith calculation point; t_x, t_y, and t_z are the rigid-body motion components; ω_x, ω_y, and ω_z the rigid-body rotation components; ε_x, ε_y, and ε_z the dilatational strain components (theoretically identical). The nine unknown coefficients can be extracted from the measured artificial displacement field using the global least-squares algorithm given in the following matrix form:

$$\mathbf{p} = \left(\mathbf{x}^T \mathbf{x}\right)^{-1} \cdot \mathbf{x}^T \cdot \mathbf{u} \tag{4}$$

where $\mathbf{p}$ is the desired artificial deformation vector $(t_x \ t_y \ t_z \ \omega_x \ \omega_y \ \omega_z \ \varepsilon_x \ \varepsilon_y \ \varepsilon_z)^T$. $\mathbf{x}$ and $\mathbf{u}$ are the matrices related to image coordinates and displacements, which can be expressed as

$$\mathbf{x} = \begin{bmatrix} 1 & 0 & 0 & 0 & z_{r1} & -y_{r1} & x_{r1} & 0 & 0 \\ \vdots & \vdots & \vdots & \vdots & \vdots & \vdots & \vdots & \vdots & \vdots \\ 1 & 0 & 0 & 0 & z_{rn} & -y_{rn} & x_{rn} & 0 & 0 \\ 0 & 1 & 0 & -z_{r1} & 0 & x_{r1} & 0 & y_{n1} & 0 \\ \vdots & \vdots & \vdots & \vdots & \vdots & \vdots & \vdots & \vdots & \vdots \\ 0 & 1 & 0 & -z_{rn} & 0 & x_{rn} & 0 & y_{rn} & 0 \\ 0 & 0 & 1 & y_{r1} & -x_{r1} & 0 & 0 & 0 & z_{r1} \\ \vdots & \vdots & \vdots & \vdots & \vdots & \vdots & \vdots & \vdots & \vdots \\ 0 & 0 & 1 & y_{rn} & -x_{rn} & 0 & 0 & 0 & z_{rn} \end{bmatrix} \quad \mathbf{u} = \begin{bmatrix} u_{r1} \\ \vdots \\ u_{rn} \\ v_{r1} \\ \vdots \\ v_{rn} \\ w_{r1} \\ \vdots \\ w_{rn} \end{bmatrix} \tag{5}$$

Since the thermally-induced artificial motion, rotation, and dilatational strain only rely on the preset imaging geometry and its variation during a scan, the extracted nine global deformation parameters can also be applied to characterize the artificial displacement and strain in the tested sample. In this regard, by subtracting the artificial displacements from the DVC-measured displacement field of the tested sample, the actual displacement arising from external loading can be recovered:

$$
\begin{bmatrix} u'_{ti} \\ v'_{ti} \\ w'_{ti} \end{bmatrix} = \begin{bmatrix} u_{ti} \\ v_{ti} \\ w_{ti} \end{bmatrix} - \begin{bmatrix} t_x \\ t_y \\ t_z \end{bmatrix} - \underbrace{\begin{bmatrix} 0 & -\omega_z & \omega_y \\ \omega_z & 0 & -\omega_x \\ -\omega_y & \omega_x & 0 \end{bmatrix}}_{Rotation} \cdot \begin{bmatrix} x_{ti} \\ y_{ti} \\ z_{ti} \end{bmatrix} - \underbrace{\begin{bmatrix} \varepsilon_x & 0 & 0 \\ 0 & \varepsilon_y & 0 \\ 0 & 0 & \varepsilon_z \end{bmatrix}}_{Dilatation} \cdot \begin{bmatrix} x_{ti} \\ y_{ti} \\ z_{ti} \end{bmatrix} \tag{6}
$$

where u_{ti}', v_{ti}', and w_{ti}' represent the corrected displacement components; u_{ti}, v_{ti}, and w_{ti} are the displacement components directly measured by DVC; x_{ti}, y_{ti}, and z_{ti} are the coordinates of the ith calculation point within the tested sample. Finally, the full-field strain results can be extracted using a pointwise least-squares algorithm [23] based on the corrected displacement field.

Experiments and Results

A rescan test and a stepwise uniaxial compression test were performed to examine the accuracy, efficacy, and practicality of the RSC method in DVC. Due to the controllable microstructure during materials forming, copper foam with 90 pores per inch and a porosity of 97.5% was chosen as the sample in the two tests. To visualize the internal microstructure, the reference and test samples at different stages were first rescanned by a Skyscan 1172 desktop X-ray micro-CT system with a spatial sampling grid of 2000 × 1336 pixels, a rotation step of 0.4°, and a voxel size of 9 μm. Note that thermal correction using a post-scan scheme [16] was applied to remove a global shift in projection images during volume image reconstruction. Next, the displacement fields of the two samples in each scan with respect to the very first scan (specified as the reference volume image) were measured by the advanced DVC method we developed recently [22]. Afterward, the RSC method was used to correct the distorted displacement fields of the test sample. Finally, the pointwise least-squares method [23] was employed to extract the full-field strains from the directly measured and corrected displacement fields. During displacement field calculation using DVC, the subvolume size was set to 51^3 voxels with a grid step of 20 voxels, and the window size for strain calculation was defined as 11 × 11 × 11 points (a local domain of 201^3 voxels).

Rescan Tests

In the rescan tests, a tested sample with a size of 11 × 11 × 8 mm^3 and a reference sample with a size of 4 × 4 × 4 mm^3 were placed on the rotation stage without external loading. To record the volume images at different operation times of the X-ray tube, CT scans were performed six times within 270 min, and each scan lasts nearly 45 min. A photo and a rendered volume image of the tested and reference samples are shown in Fig. 4.

The DVC-measured displacement fields within the tested sample in the last stage (i.e., the displacement between stage 6 and stage 1) before and after systematic error correction using the RSC method in the rescan tests are shown in Fig. 5. We can make two conclusions from Fig. 5. First, the directly measured displacement fields (i.e., U, V, and W) show significant bias (or systematic error) and fluctuation due to artificial displacements and strains. From the inserted values, the maximum mean bias and standard deviation (SD) of the directly measured displacements are −1.0768 voxels and 0.0890 voxels, respectively. The corrected displacement results are close to 0,
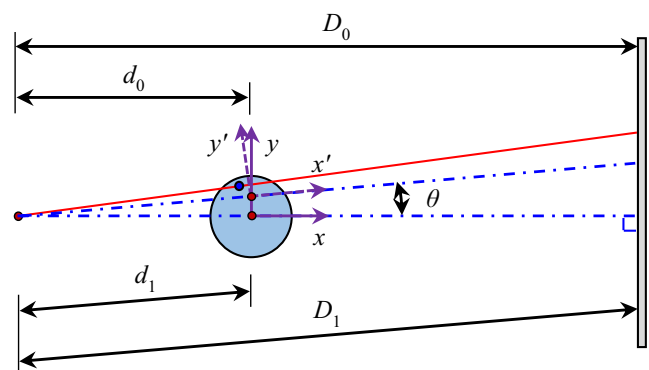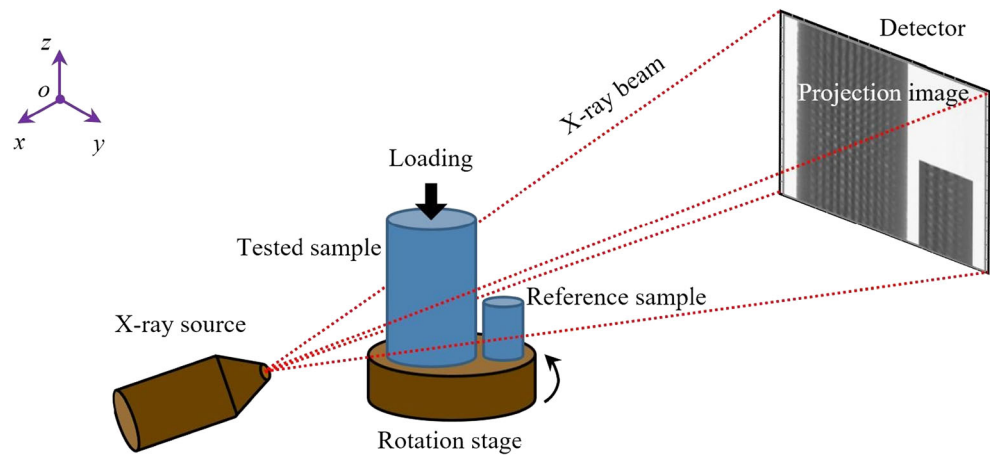
Fig. 2 Changes in imaging geometry of a lab-CT due to rotation of X-ray beam

Fig. 3 Schematic diagram showing the experimental setup of the RSC method employed in DVC

Uniaxial Compression Tests

The experimental setup of the stepwise uniaxial compression test is illustrated in Fig. 7. Before image scanning, a small reference sample with a size of $5 \times 5 \times 5$ mm^3 was attached beside the tested counterpart with a size of $10 \times 10 \times 10$ mm^3. A preset compression load of 100 g was exerted on the tested specimen to ensure the stability of stepwise loading and volumetric imaging. The stepwise displacements exerted on the test sample were set as 0.01 mm, 0.02 mm, and 0.03 mm along the z direction. After reaching the preset displacement in each step, a CT scan was performed to record the volume images at the current state. In total, four scans were performed within 180 min, and the duration of each scan was approximately 45 min.

Figure 8 displays the measured z-displacement fields within the tested sample before and after systematic error correction in the stepwise uniaxial compression test. Since the self-heating effect induces significant systematic errors in DVC-measured displacements and strains, the measured W displacement fields in the top row of Fig. 8 show a smaller deformation range along the z direction, and mean strains dramatically deviate from prescribed values. In contrast, the corrected displacement fields show significant differences in the contour levels and mean strains closer to the imposed deformations. Thus, it can

with a maximum mean bias of 0.0009 voxels and a maximum SD of 0.0203 voxels, which agree well with the real zero-deformation case. Second, the uncorrected displacement fields exhibit significant expansion in the x, y, and z directions, and the artificial normal strains are estimated as 339.6 µε, 367.4 µε, and 346.9 µε, respectively. These strains can be regarded as thermally-induced dilatational strains. In contrast, the dilatational strains in the corrected displacement fields are negligibly small values that are less than 20 µε. By comparison, the artificial displacements and strains due to the self-heating effect of the X-ray tube can be effectively eliminated after employing the RSC method.
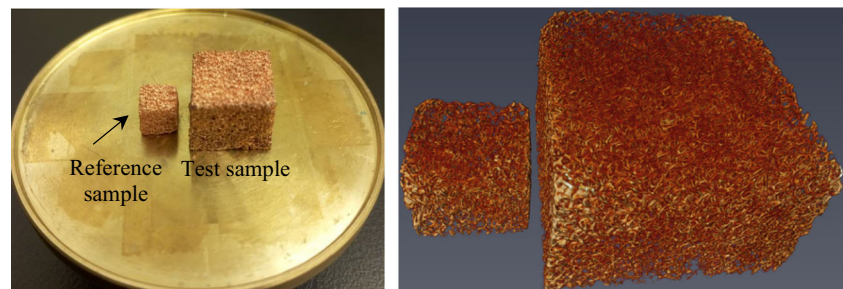
Based on the DVC-measured displacement fields before and after correction, mean values of the three displacement components and three normal strain components can be extracted. Figure 6 depicts the systematic errors of the displacements and strains within the tested sample before and after using the RSC method in the rescan tests. It can be observed that: (1) both the measured displacement and strain components increase with system uptime, and then tend to certain asymptotic values; (2) the systematic errors in displacements and strains reach 1.2 voxels and 370 µε at the end, but decrease to less than ±0.02 voxels and ±20 µε after employing the RSC method; and (3) the accuracy of the presented RSC method can be identified as 0.02 voxels for displacement and 20 µε for strain in this rescan tests.

Fig. 4 Photo (left) and rendered volume image (right) of the reference and test samples
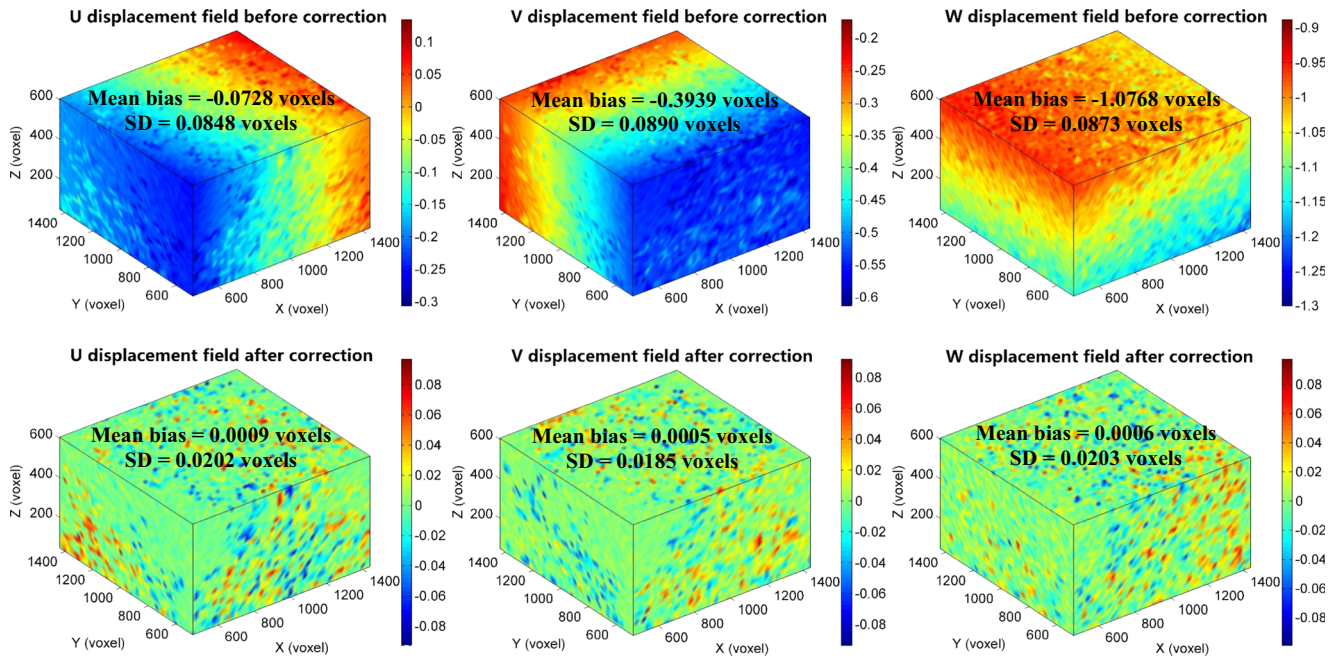
Fig. 5 DVC-measured displacement fields within the tested sample before (upper) and after (lower) systematic error correction: (left) *u* displacement field, (middle) *v* displacement field, (right) *w* displacement field

be concluded that the presented RSC method can effectively remove the systematic errors and recover the actual deformation.

For comparison, Fig. 9 illustrates the imposed strain-stress curve (solid line) along with the averaged values of the directly measured strains (red dots) and the corrected results (blue squares) of the test sample before and after using the RSC method. The directly measured and corrected strain values as well as their corresponding errors are shown in the inserted table for quantitative comparison. It is seen that the directly measured average strains show evident deviations from the imposed ones. Their differences increase with the number of loading stages, and the maximum bias error exceeds 300με in stage 3. By contrast, the corrected strains show good agreement with the loading configuration, and exhibit negligibly small bias errors (less than 20 με).

It should be noted that a larger imaging magnification may amplify the detrimental influence of the self-heating effect,
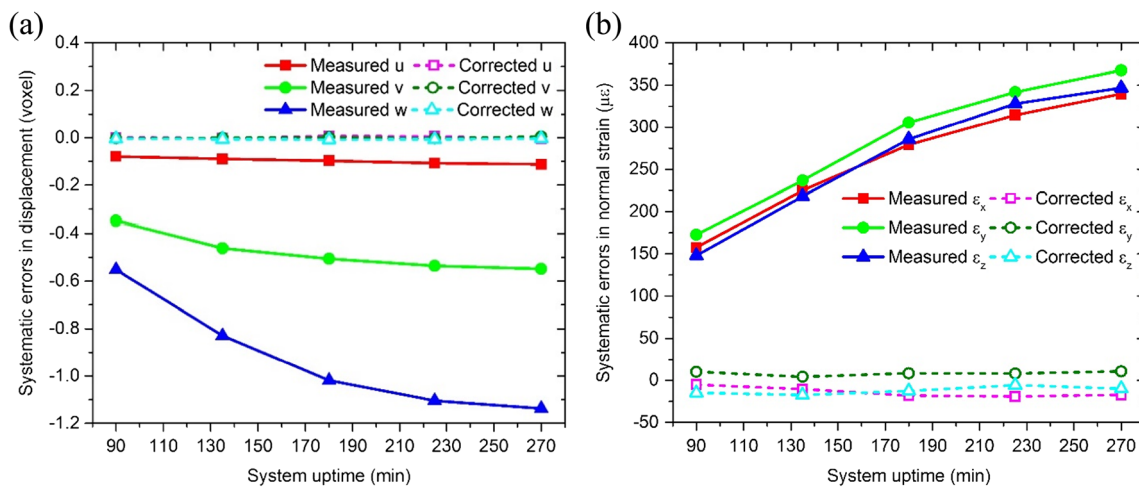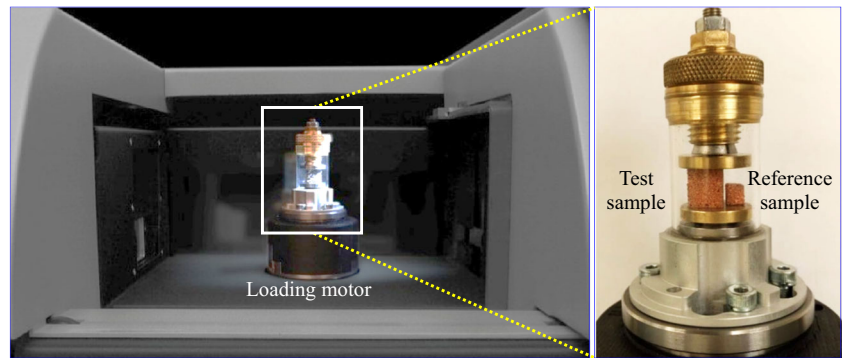

Fig. 6 Systematic errors of the DVC-measured (**a**) displacement components and (**b**) normal strains within the tested sample before and after performing RSC method in the rescan tests

Fig. 7 Setup of the stepwise uniaxial compression test of copper foam sample

and hence much larger systematic error (more than 0.4% dilatational strain) may be present. In this case, the use of the proposed RSC method is expected to be more effective in correcting thermally-induced systematic errors and improving the accuracy of DVC measurements.

Discussion

By using a stationary reference sample placed adjacent to the test sample, the proposed RSC method can effectively remove the detrimental artificial displacements and strains associated with the self-heating effect of X-ray scanners. Compared with past solutions [14–17, 19–21], the proposed RSC method can be easily implemented to realize *in-situ* systematic error correction. Since the reference sample is used to monitor the artificial displacements due to the instability of an imaging system, the reference sample need not consist of the same material as the test sample. In practical implementation, a cheap and easily available material with identifiable internal texture and near-zero thermal expansion coefficient is highly recommended.
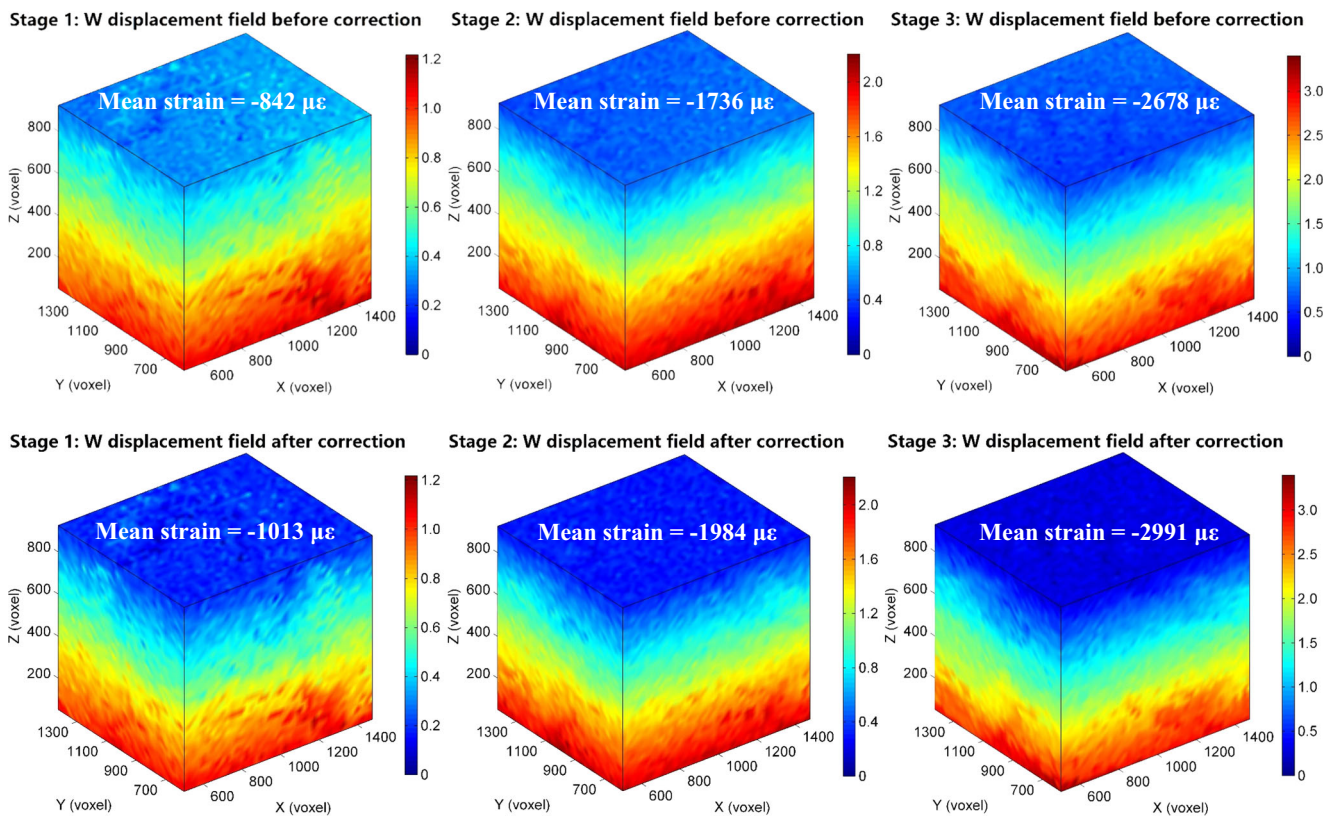

Fig. 8 W displacement fields within the tested sample before (upper) and after (lower) systematic error correction: (left) 0.1% strain, (middle) 0.2% strain, (right) 0.3% strain
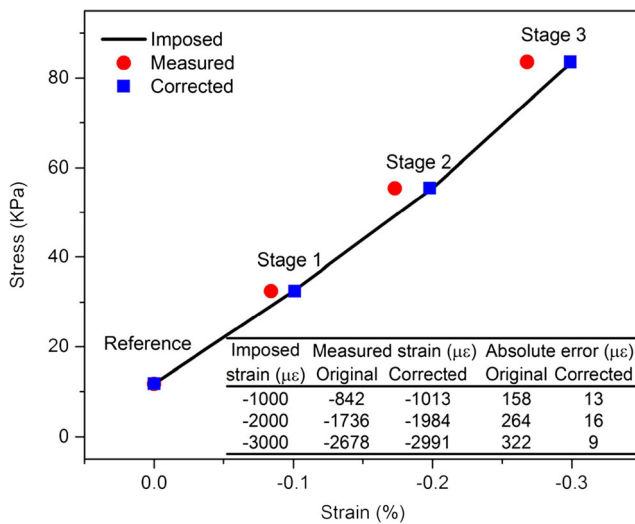
Fig. 9 Preset strain-stress curve and the average strain of the test sample before and after performing the RSC method in the stepwise uniaxial compression test. The inserted table shows the corresponding strain values and absolute errors

different sizes (i.e. $100 \times 100 \times 100$ voxels, $200 \times 200 \times 200$ voxels, $400 \times 400 \times 400$ voxels) are selected within the reference samples in the 2nd and 4th CT scans in the rescan tests. Note that the subvolume size is selected as $51 \times 51 \times 51$ voxels with a grid step of 20 voxels. The extracted artificial displacements and dilatational strains are listed in Table 2. It is seen that there are slight differences in the extracted artificial deformation components when selecting different VOI sizes (representing diverse sizes of reference sample). The maximum bias in detected displacements and strains are less than 0.01 voxels and 20 $\mu\varepsilon$, respectively, even though the VOI is selected as small as $100 \times 100 \times 100$ voxels ($0.9 \times 0.9 \times 0.9$ mm) comprising $6 \times 6 \times 6$ calculation points. Although different VOIs result in almost identical artificial deformation components, a relative large reference sample is preferable in practice to ensure data robustness during global fitting.

Conclusion

DVC in combination with laboratory X-ray CT scanners has been recognized as a powerful technique for quantifying interior deformation of various opaque solids and biological materials. The self-heating effect of the X-ray tube within a CT scanner has been identified as the most detrimental factor in DVC measurements. In this work, the geometric relationship between the thermal drift of the emission point due to the self-heating effect and the induced artificial deformation in volume images is derived theoretically. A simple and effective RSC method is proposed for *in-situ* systematic error correction to realize high-accuracy internal deformation measurement using DVC and an X-ray scanner. A series of rescan tests and a stepwise uniaxial compression test of a cubic copper foam sample successfully demonstrated the efficacy and practicality of the proposed RSC method. Experimental results indicate that this method can reduce thermally-induced artificial displacements and strains to negligible levels. Because the proposed method can easily and effectively achieve *in-situ* systematic error correction, it is expected to be used in various DVC applications requiring high measurement accuracy.

Despite offering the advantages of *in-situ* error correction with easy operation, the RSC method is not without its limitations. To be specific, the spatial resolution available for the tested sample is reduced when using the proposed RSC method, because the reference sample will occupy a certain portion of the field of view. Thus, if one intends to maximize the spatial resolution of a test sample, the proposed RSC method is no longer applicable. In this case, other techniques, e.g., full preheating of the X-ray scanner or post-correction based on a pre-calibrated artificial strain-time curve, can be employed.

Also, it should be noted that the size of the reference sample and the specific calculation parameters may influence the efficacy and accuracy of the proposed compensation method. In this work, a global least-squares fitting method is applied to the DVC-measured displacement fields of the reference sample to extract the artificial deformation components. Since the deformation field in the reference sample is almost homogeneous and can be characterized by a simple trilinear function, a large strain calculation window (i.e., more plentiful displacement data) is preferred due to its better noise-proof performance. To quantify the influence of the size of the reference sample on estimated artificial displacements, VOIs with three

Table 2 The extracted artificial displacement components and dilitational strain during implementing the proposed RSC method using different VOI sizes in the rescan tests

VOI size (voxel)	2nd scan				4th scan			
	u (voxel)	v (voxel)	w (voxel)	ε ($\mu\varepsilon$)	u (voxel)	v (voxel)	w (voxel)	ε ($\mu\varepsilon$)
$400 \times 400 \times 400$	−0.074	−0.367	−0.545	149.3	−0.093	−0.540	−1.007	250.2
$200 \times 200 \times 200$	−0.078	−0.364	−0.548	153.2	−0.097	−0.539	−1.001	256.0
$100 \times 100 \times 100$	−0.082	−0.364	−0.538	143.3	−0.089	−0.535	−0.999	261.9

Appendix

Here we theoretically analyze the relationship between rotation of X-ray optical axis and the induced artificial deformations in reconstructed volume images. By comparing with the ideal case, the change in imaging geometry due to rotation of X-ray optical axis can be decomposed into three aspects: (1) motion of emission point in Fig. 10(a), (2) rotation of sample in Fig. 10(b), (3) eccentric rotation of detector in Fig. 10(c).

First, the motion of emission point along y direction shown in Fig. 10(a) causes rigid-body translation v_2 in the volume image as discussed above.

$$v_2 = -\left(\frac{D_1}{d_1} - 1\right) \cdot d_0 \tan\theta = -\left(\frac{D_0}{d_0} - 1\right) \cdot d_0 \tan\theta \quad (7)$$

Second, since the direction of X-ray beam deviates from ideal case, X-ray beam passes through the sample along different paths. As such, the difference from ideal beam path can be equivalent to a rotation of the sample with an angle of θ, thus finally causing a rigid-body rotation θ of volume image. Third, the rotation of detector around point O' first includes a deviation of the rotation center, thus a rigid-body translation v_3 from O to O' may be present in the reconstructed volume image.

$$v_3 = \left(\frac{D_0 - d_0}{d_0}\right) \cdot d_0 \tan\theta \quad (8)$$

From the above two expressions, v_2 and v_3 are equal but in opposite directions, thus rotation of X-ray beam causes no rigid-body translation in the volume image. Also, since the detector deviates from the ideal direction (i.e., perpendicular to the X-ray beam), the upper part of the projection image may expand due to the increased amplification, while the lower part shrinks. As a result, a complex non-uniform deformation may occur within the reconstructed volume image due to the rotation of detector according to the commonly-used Feldkamp algorithm in a lab cone-beam CT system. The corresponding theoretical analysis is detailed as follows.
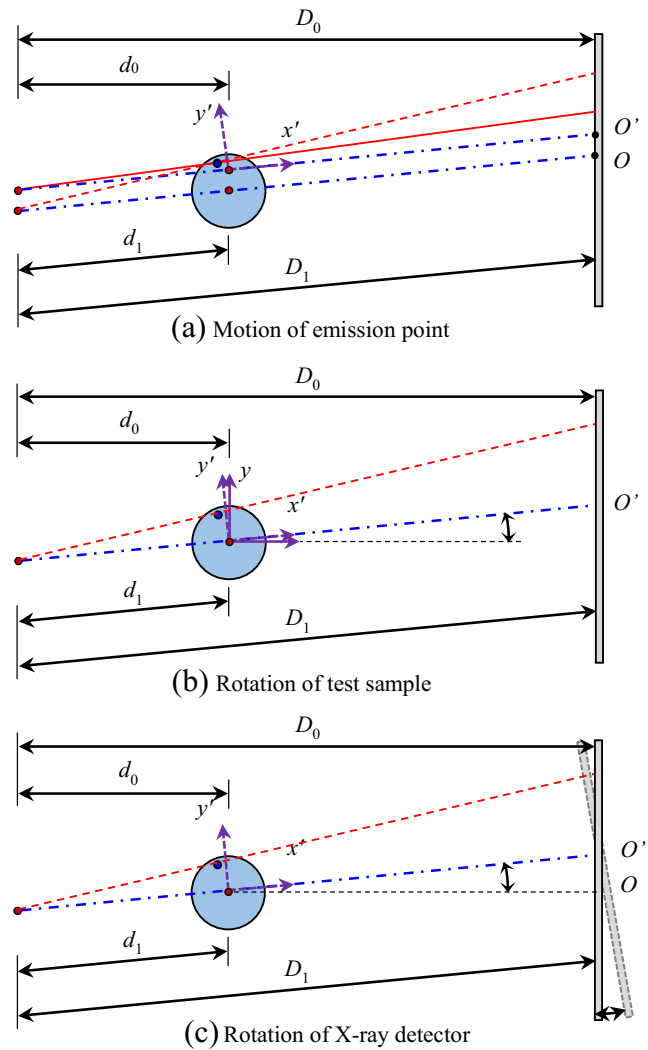

(a) Motion of emission point

(b) Rotation of test sample

(c) Rotation of X-ray detector

Fig. 10 Decomposition of the changes in imaging geometry of a lab-CT due to rotation of X-ray beam: (**a**) motion of emission point, (**b**) rotation of sample, (**c**) eccentric rotation of detector

As illustrated in Fig. 11(a), assume the perpendicular distance from rotation center to the X-ray cone-beam is Y, the projection image $P_\Phi(Y)$ can be denoted as a function of Y and rotation angle Φ of the sample. In ideal case, the detector should be perpendicular to the X-ray beam, then we can get the projected position y as follows

$$y = \frac{Y}{d_1} \cdot D_1 \quad (9)$$

While the projected position y' on rotated detector can be expressed as

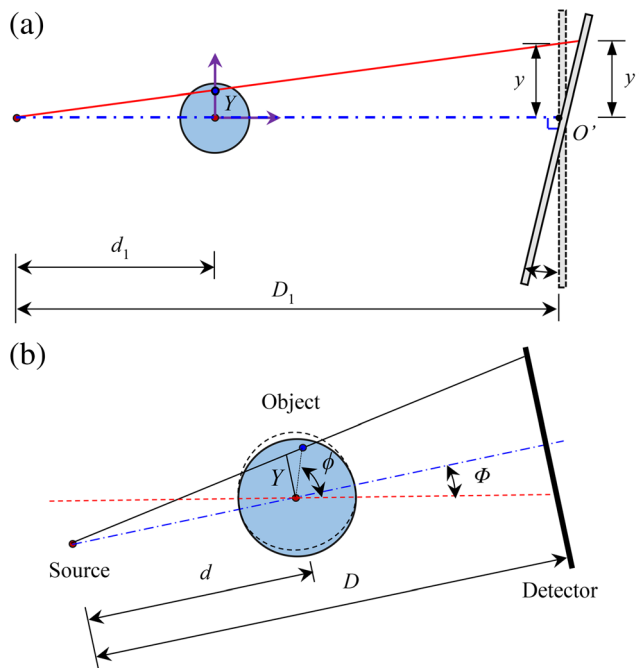$$y' = \frac{D_1 Y}{d_1 - Y \tan\theta} \quad (10)$$

Fig. 11 (**a**) Equivalent imaging geometry due to the rotation of X-raydetector, and (**b**) the resulting image deformation

Then, the corresponding position Y' should be written as

$$Y' = \frac{y'}{D_1} \cdot d_1 = \frac{Yd_1}{d_1 - Y\tan\theta} \quad (11)$$

From the above expression, it is seen that the distance Y shared by the points along X-ray beam may change to Y' due to the rotation of detector. In this regard, the effect of X-ray detector rotation can be equivalently described as: as for each rotation angle Φ of the test sample, the upper part of the sample (above optical axis) expand, while the lower part (below optical axis) shrink as exhibited in Fig. 11(b). As such, the final intensity or position changes in volume images highly depends on specific algorithm employed during volume image reconstruction. In most cases, however, these non-uniform deformations are limited to far less than 1 voxel and present as random intensity changes rather than a global bias, thus can be considered as random errors rather than systematic errors.

References

1. Bay BK, Smith TS, Fyhrie DP et al (1999) Digital volume correlation: three-dimensional strain mapping using X-ray tomography. Exp Mech 39(3):217–226
2. Bay BK (2008) Methods and applications of digital volume correlation. J Strain Anal. Eng 43(8):745–760
3. Roberts BC, Perilli E, Reynold KJ (2014) Application of the digital volume correlation technique for the measurement of displacement and strain fields in bone: a literature review. J Biomech 47(5):923–934
4. Fedele R, Ciani A, Fiori F (2014) X-ray microtomography under loading and 3D-volume digital image correlation. A review. Fund Inform 135(1–2):171–197
5. Pan B, Qian KM, Xie HM, Asundi A (2009) Two-dimensional digital image correlation for in-plane displacement and strain measurement: a review. Meas Sc Technol 20:062001
6. Jandejsek I, Jiroušek O, Vavřík D (2011) Precise strain measurement in complex materials using digital volumetric correlation and time lapse micro-CT data. Proced Eng 10:1730–1735
7. Pan B, Wang B, Wu D, Lubineau G (2014) An efficient and accurate 3D displacements tracking strategy for digital volume correlation. Opt Laser Eng 58:126–135
8. Maire E, Withers PJ (2014) Quantitative X-ray tomography. Int Mater Rev 59(1):1–43
9. Buffiere JY, Maire E, Adrien J, Masse JP, Boller E (2010) In situ experiments with X-ray tomography: an attractive tool for experimental mechanics. Exp Mech 50(3):289–305
10. Toda H, Maire E, Aoki Y, Kobayashi M (2011) Three-dimensional strain mapping using in situ X-ray synchrotron microtomography. J Strain Anal Eng 46(7):549–561. https://doi.org/10.1177/0309324711408975
11. Réthoré J, Limodin N, Buffiere JY, Hild F, Ludwig W, Roux S (2011) Digital volume correlation analyses of synchrotron tomographic images. J Strain Anal Eng 46(7):683–695. https://doi.org/10.1177/0309324711409999
12. Davis GR, Elliott JC (2006) Artefacts in X-ray microtomography of materials. Mater Sci Technol 22(9):1011–1018
13. Boas FE, Fleischmann D (2012) CT artifacts: causes and reduction techniques. Imaging in Medicine 4(2):229–240
14. Limodin N, Réthoré J, Adrien J, Buffière JY, Hild F, Roux S (2011) Analysis and artifact correction for volume correlation measurements using tomographic images from a laboratory X-ray source. Exp Mech 51(6):959–970
15. Wang B, Pan B, Tao R, Lubineau G (2017) Systematic errors in digital volume correlation due to the self-heating effect of a laboratory X-ray CT scanner. Meas Sci Technol 28:055402
16. Salmon PL, Liu X, Sasov A (2009) A post-scan method for correcting artefacts of slow geometry changes during microtomographic scans. J X-ray Sci Technol 17(2):161–174
17. Sun W, Brown S, Flay N, McCarthy M, McBride J (2016) A reference sample for investigating the stability of the imaging system of X-ray computed tomography. Meas Sci Technol 27(8):085004
18. Pan B, Yu L, Wu D (2013) High-accuracy 2D digital image correlation measurements using low-cost imaging lenses: implementation of a generalized compensation method. Meas Sci Technol 25(2):025001
19. Flay N, Sun W, Brown S, Leach R, Blumensath T (2015) Investigation of the focal spot drift in industrial cone-beam X-ray computed tomography. Digital industrial radiology and computed tomography (DIR 2015), Ghent, 22–25 Jun 2015
20. Hiller J, Maisl M, Reindl LM (2012) Physical characterization and performance evaluation of an x-ray micro-computed tomography system for dimensional metrology applications. Meas Sci Technol 23(8):085404
21. Vogeler F, Verheecke W, Voet A, Kruth JP, Dewulf W (2011)Positional stability of 2D x-ray images for computer tomography. Int. symposium on digital industrial radiology and computed tomography, berlin, 20–22 June 2011
22. Pan B, Wang B (2017) A flexible and accurate digital volume correlation method applicable to high-resolution volumetric images. Meas Sci Technol 28(10):105007
23. Pan B, Wu D, Wang Z (2012) Internal displacement and strain measurement using digital volume correlation: a least-squares framework. Meas Sci Technol 23(4):045002